Biomass-derived porous carbon materials with NiS nanoparticles for high performance supercapacitors

Huafang Yang[1,2], Yinghua Tang[1,2], Xiaoyan Sun[1,2], Quan Liu[1,2], Xiaogu Huang[1,2,3], Lixi Wang[1,2], Zhenxiao Fu[4,5,6],Qitu Zhang[1,2*], Siu Wing Or[3*]

[1] College of Materials Science and Engineering, Nanjing Tech University, Nanjing 210009, China

[2] Jiangsu Collaborative Innovation Center for Advanced Inorganic Function Composites, Nanjing 210009, China

[3] Department of Electrical Engineering, the Hong Kong Polytechnic University, Hung Hom, Kowloon, Hong Kong

[4] State Key Laboratory of Advanced Materials and Electronic Components, Nanjing 210009, China

[5] Fenghua Research Institute (Guangzhou) Co. Ltd., Guangzhou, China

[6] Guangdon Fenghua Advanced Technology Company Limited, Zhaoqing 526020, China

[*]Corresponding authors.

E-mail addresses: ngdzqt@163.com (Qitu Zhang), eeswor@polyu.edu.hk (Siu Wing Or)

Tel: 086-25-83587246(Qitu Zhang), 852-34003345(Siu Wing Or)

Abstract 3D nanoparticles were synthesized by facile hydrothermal method with the hexamethylenetetramine as soft templates. The effects of reaction temperature and time on electrochemical properties were seriously studied in this research. The optimal specific capacitance 1688.5F g^{-1} at the current density of 1A g^{-1} was obtained when the temperature is 180°C and reaction time is 8h. Through combining the nanoparticles with the natural biomass carbon materials, the 3D open-pore silk ribbon like architecture is acquired when the carbonization temperature of the walnut shell is 600°C. Electrochemical studies manifest that the NiS/C-600 composites have better electrical conductivity and electrochemical rate performance. The final satisfactory

electrochemical behaviors deprived from the introduction of walnut shells opens a novel route of biomass carbon electrode materials for excellent performance energy device.

1 Introduction

With the continuous consumption of fossil fuels and the caused environmental deterioration, the demand for seeking renewable and clean energy sources become more and more urgent[1-3]. Among the various energy and conversion devices, the supercapacitors not only possess the high energy density of secondary batteries but also own the high power density of capacitors[4]. It is prospective to solve the energy and pollution problems due to the remarkable characteristics. According to the energy storage mechanisms, electrochemical supercapacitors can be classified into two categories. They are the electric double layer capacitors(EDLCs) greatly influenced by the surface area such as porous carbon materials[5], graphene[6] and carbon nanotubes[7], and the pseudocapacitors mainly depending on the pseudo-Faradaic process. Composed with the EDLCs, the pseudocapacitors show higher specific capacitiance because of the additional fast and reversible redox reactions between active materials and electrolyte ions[8]. However, it has the inferior cycling stability due to the degradation of the active materials. Considering a win-win situation, the EDLCs and the pseudocapacitor need to work together to acquire practical products[9].

Recently, transition metal sulfides such as FeS_2[10], CoS[11], NiS[12], CuS[13] and ZnS[14] have attracted tremendous attention due to the low energy band gap as well as good electrical conductivity, long cycle life and high specific capacitance. Of the different metal sulfides, the nickel sulfides are more favorable because of its high

redox activity, low cost, simple fabrication and high theoretical capacity[15]. It is reported that nickel sulfides with various phases including NiS[16], Ni_3S_2[17], NiS_2[18], Ni_3S_4[19] and Ni_7S_6[20] have been widely investigated and present high capacitive performance and good cycling stability. Unfortunately, the low surface area and nonporosity of nickel sulfides limit the diffusivity of electrons, thus restricting contribution of capacitance[21]. To solve these problems, various nickel sulfide-based microstructures have been synthesized. For example, Wang et al synthesized nickel sulfide/graphene oxide nanocomposite and achieved a high specific capacitance of 800F g^{-1} at the current density of 1A g^{-1}[22]. Li et al grew nickel sulfide on graphene-covered make-up cotton by "dip and dry" and electrodeposition methods and the MCs based on GNS/NiS hierarchical nanostructures could exhibit a specific capacitance of 775F g^{-1} at a current density of 0.5A g^{-1}[23]. Yu et al prepared interconnected and staggered nickel sulfide nanosheets supported by nickel foam via an ultrasound-assisted soaking method using nickel hydroxide nanosheets as precursor and the unique structure exhibited excellent electrochemical performance, including high area capacitances (2.64F cm^{-2}) and remarkable cycling stability (90% retaining after 2000 cycling)[24]. Nevertheless, there is still much room to improve the specific capacity and cycle stability. In addition, these processes to fabricating nickel sulfide-based electrodes are relatively complicated. Hence, it is still a big challenge to gently synthesize porous morphological NiS-based materials for supercapacitors with high performance.

So far, many natural biomass-derived carbon materials have been applied for electrochemical energy storage such as cotton[25], peanut shells[26], beans shells[27], loofah sponge[28], tea[29] and rice husks[30, 31]. They exhibit excellent electrochemical performance because the naturally porous or hierarchical structures

can reduce the ion diffusion distance and heteroatoms will provide extra active sites[32]. Moreover, the biomass-derived carbon materials are mainly from agricultural wastes which overcome the shortcomings of costly and complicated preparation process in nanostructured carbons. Walnut shells are one of the common renewable biomass resources, which are cheap and easily available. To our knowledge, walnut shells have been widely used for various devices, but rarely applied for supercapacitors. Herein, we firstly prepared the NiS nanoparticles by a facile hydrothermal method under different reaction temperatures and reaction times. The maximum specific capacitance of 1688.5F g^{-1} at current density of 1A g^{-1} is acquired when reaction temperature and time are 180°C and 8h. In order to enhance the conductivity and electrochemical stability of NiS nanoparticles, we cooperated the NiS nanoparticles with walnut shell-derived carbon materials to relieve the specific capacitance attenuation with respect to scan rates. The resulting NiS/C-600 composites show a relative high specific capacitance of 1518.3F g^{-1} at 1A g^{-1}, and good capacitive retention of 96.08% after 1000 cycles.

2 Experimental

2.1 Materials

Walnut shells were obtained from local market in Nanjing(China). All other reagents were of analytical-grade reagents and used without further purication except otherwise stated. All the solution was prepared using de-ionized (DI) water.

2.2 Preparation of NiS / Walnut shell

Typically, the synthesis of NiS/walnut shell composites were carried out as follows. Firstly, the KOH treated walnut shells were heated in the tube furnace at the

rate of 5°C/min to 500, 600, 700 and 800°C respectively and maintained at this temperature for 2h under N_2 atmosphere, yielding black powders. Then, under vigorous magnetic stirring, 30.0mL aqueous solution containing 3.0mmol $Ni(NO_3)_2 \cdot 6H_2O$, 3.0mmol hexamethylenetetramine and 12.0 mmol thiourea were added 50.0mg 500, 600, 700 and 800°C heated walnut powders respectively. The samples were donated as NiS/C-500, NiS/C-600, NiS/C-700 and NiS/C-800. The sample was mixed completely and then transferred into Teflon-lined stainless steel autoclave and heated under a certain temperature and time. After the reaction was completed, the autoclave cooled to room temperature naturally. Precipitates were centrifuged, sequentially washed with water for several times to remove the ions possibly remaining in the products, and finally dried in a vacuum oven at 60°C for 12h. The NiS nanoparticles were prepared using the same route in the absence of walnut shell-carbons.

2.3 Characterization

The crystalline phases were characterized by X-ray diffraction (XRD, smartlabTM 9kW, Rigaku, Japan) using Cu Kα radiation (λ=1.5406Å) in the range of 5–80° with step size 0.02° and scanning rate 5°/min. The morphology of the samples were measured by scanning electron microscopy (SEM, Hitachi, Japan). High-resolution transmission electron microscopy (HRTEM, Tecnai-G20, FEI) was carried out with an accelerating voltage of 200kV. X-ray photoelectron spectroscopy(XPS, K-Alpha, Thermo Fisher Scientific) measurements were taken on with a monochromatic Al Ka (1486.6eV) as X-ray source. Raman spectra were collected using a Raman spectrometer (Labram HR800, Japan) with a 514nm laser beam as the light source.

2.4 Fabrication of the electrode and electrochemical measurements

All electrochemical measurements were performed on a CHI660E electrochemical workstation in a conventional three-electrode system with 2M KOH solution as the electrolyte. The three-electrode cell was made up of platinum sheet as counter electrode, saturated calomel electrode (SCE) as reference electrode and active materials as a working electrode. The working electrodes were employed with casting mixtures of 70wt% active materials containing 20wt% acetylene black and 10 wt% polyvinylidene fluoride (PVDF) on nickel foam (1cm×1cm). The electrochemical performance was carrying out using cyclic voltammetry (CV), galvanostatic charge–discharge tests (GCD), and electrochemical impedance spectroscopy (EIS) measurements (1–100,000 Hz).

3. Results and discussion

3.1 Characterizations of NiS

The XRD patterns of NiS synthesized at different temperatures and times are shown in Fig. 1. Ten apparent diffraction peaks at 30.17°, 34.74°, 46.03°, 53.55°, 60.90°, 62.73°, 65.70°, 70.78°, 73.33° and 79.08° are presented and can be identified for the (100), (101), (102), (110), (103), (200), (201), (004), (202) and (104) planes of the hexagonal phase of NiS(JCPDS No. 02-1280) with lattice parameters a = 3.41Å, c = 5.32Å respectively. The other diffraction peaks at 18.44°, 32.21°, 35.70°, 37.34°, 40.45°, 48.84°, 50.14°, 52.64°, 56.25°, 57.41° and 59.73° respectively correspond to (110), (300), (021), (220), (211), (131), (410), (401), (321), (330) and (012) planes of the rhombohedral NiS (JCPDS No. 12-0041) crystalline structure. The results indicate that the electrode materials are composed of two phases and no other impurity peaks can be observed when the temperature is 180°C and the time is 8h.

As can be seen from Fig. 1(a), the peak width at half height of the diffraction peaks at (100), (101), (102) and (110) are obviously larger than other diffraction peaks when the temperature is lower than 180°C. It shows that the crystallinity is low and the organic reactants were not completely reacted. When the temperature increases to 200°C, the peaks intensity of the second phase become larger indicating the high degree of crystallization. Therefore, the samples synthesized at 180°C may

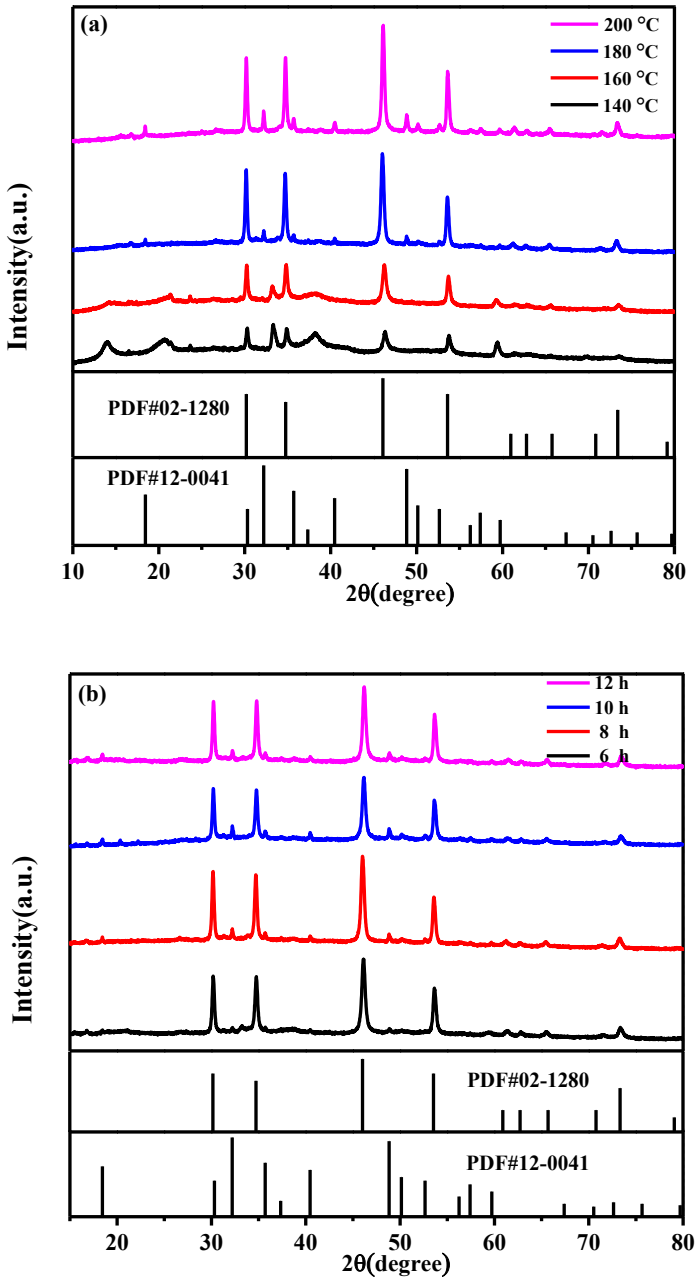

Fig.1. XRD spectra of NiS at (a) different temperatures from 140°C to 200 °C under the condition of 8h, (b)different hours from 6 to 12h under the condition of 180 °C.

be more suitable for super-capacitor materials. Fig. 1(b) displays XRD spectra of NiS at different reaction times and no impurity peaks are observed. The SEM images of the samples with different reaction temperatures and times are shown in Fig. 2(a–h). It can be seen that the NiS particles become larger and distribution of particle size is uneven as the reaction time grows longer(>8h). It shows the length of reaction time can also affect the microstructure of the samples. When the hydrothermal reaction temperature increases to 200°C, the reunion phenomenon of NiS particles become more serious. In addition, the particles are entangled with each other when the temperature is low(<180°C). The sample of NiS nanoparticles possess loose and porous structure with uniform size of 200nm when the temperature is 180°C and the time is 8h. As a result, this reaction conditions are chosen to synthesize NiS electrode materials because the porous structure not only benefits the diffusion of the electrolyte between the hole, but also provides a good transmission channel and large storage space for the electrolyte ions which can improve the electrochemical performance.

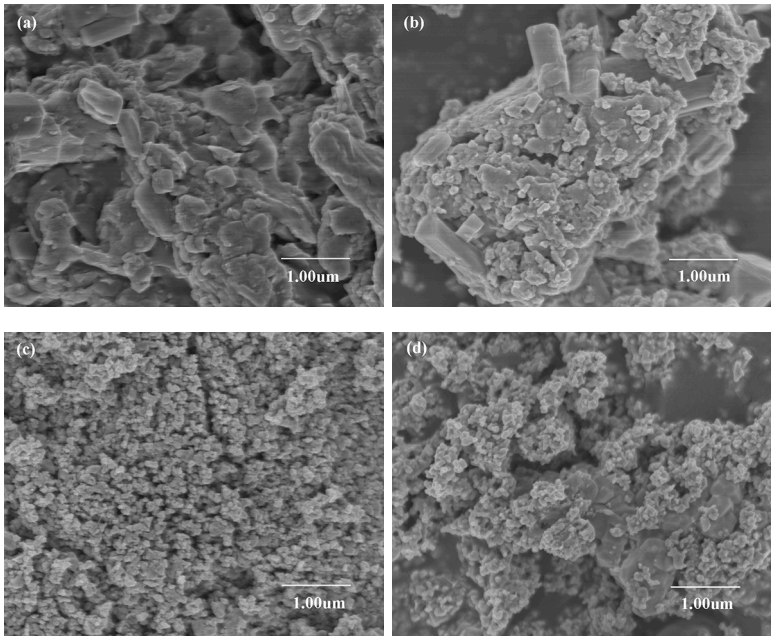

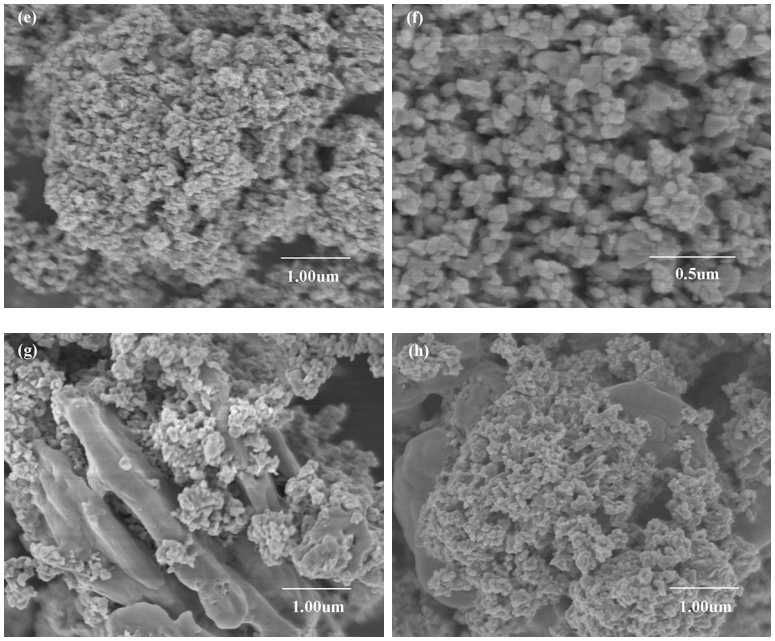

Fig.2.SEM images of NiS particles (a-d) different temperatures (140, 160, 180 and 200^{o}C)under the condition of 8h, (e-h)different hours (6, 8, 10 and 12h) under the condition of 180 ^{o}C.

X-ray photoelectron spectroscopy (XPS) measurements were used to analyze the surface chemical state of NiS particles. Fig. 3(a) displays the survey spectrum of NiS particles which indicates the peaks of Ni, S, C, and O. With the Gaussian fitting method, the Ni 2p spectrum shown in Fig.3(b) is fitted to two spin-orbit doublet peaks and two shake-up satellites. The binding energies of the $Ni2p_{3/2}$ peaks are observed at 853.4 and 856.23eV and the $Ni2p_{1/2}$ peaks are shown at 870.65 and 873.84eV. Moreover, the peaks at 853.4 and 870.65eV are the characteristic of Ni^{2+} and the peaks at 856.23 and 873.84eV correspond to Ni^{3+}[33]. The satellite peaks at 861.75 and 879.61eV are attributed to nickel-oxygen species on the surface of the NiS nanoparticles. On the other hand, the XPS spectrum of S2p is demonstrated in Fig.3(c). The peak located at 163.08eV corresponds to the metal sulfide which indicates the presence of S^{2-} in NiS materials, while the binding energy at 161.86eV can be owed to the sulfur ion in low coordination at the surface[34]. Generally, the well-matched peaks further confirm the state of Ni and S in the NiS nanoparticles.

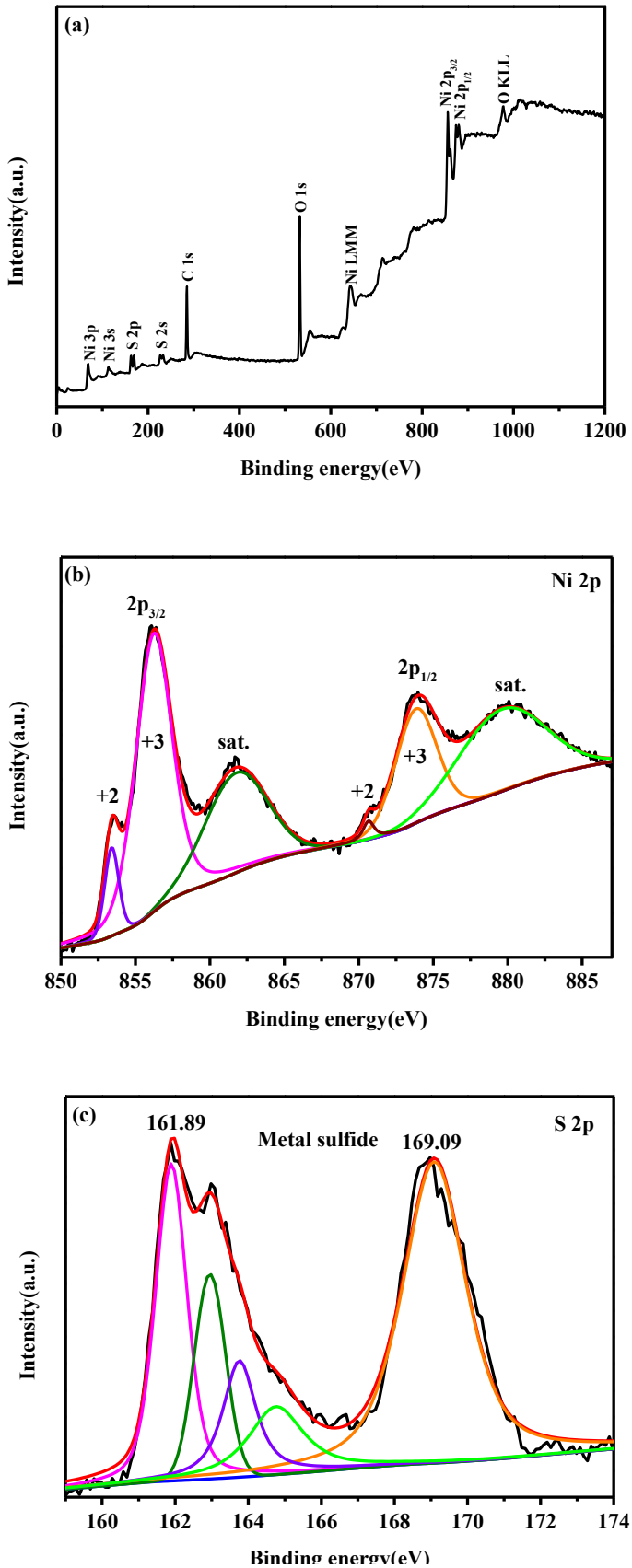

Fig.3.XPS spectrum of NiS particles (a) XPS survey spectrum, (b)Ni 2p spectrum, (c) S 2p spectrum.

Fig.4(a-d) shows the SEM images of NiS/C-500, NiS/C-600, NiS/C-700 and NiS/C-800. It can be seen that the NiS/C-600 composites are composed of numerous nanosheets that construct interconnected 3D open network-like microstructure. The porous and loose structure can provide more electroactive sites for electrochemical reactions. Combined with the biomass carbon materials, the NiS nanoparticles are protected from pulverization. Moreover, the NiS nanoparticles can prevent the agglomeration of prepared carbon materials, thus the utilization of pseudocapacitance in NiS/C-600 can be improved greatly. However, the NiS/C-500, NiS/C-700 and NiS/C-800 composites reunite seriously and result to poor transportation of electrolyte ions which can explain the inferior electrochemical performance. TEM measurements were conducted to further explore the structure of NiS/C-600 nanosheets and the images are shown in Fig. 4(e-f). The silk ribbon like sheets are made up of nanoparticles of 50nm. Obviously, the lattice fringe with a lattice spacing of ~ 0.48nm corresponds to the (110) plane of NiS phase.

Fig.4.(a-d)SEM images of NiS/C-500, NiS/C-600, NiS/C-700 and NiS/C-800, (e-f)TEM images of NiS/C-600.

The Raman spectra of NiS/C-600 structure are shown in Fig.5. Two strong peaks located at 1350cm^{-1} and 1590cm^{-1} are corresponding to D bond and G bond[35]. The D bond originates from the breathing mode of *k*-point phonons of A_{1g} symmetry and indicates defects and disordered carbonaceous structure of the activated materials[36]. The G band represents the E_{2g} phonon of sp^2 carbon atoms. The I_D/I_G intensity ratio of NiS/C-600 is 1.02, suggesting a high percentage of disorder and porous structure which benefit the transportation/diffusion of electrolyte ions and favour the electrochemical performances.

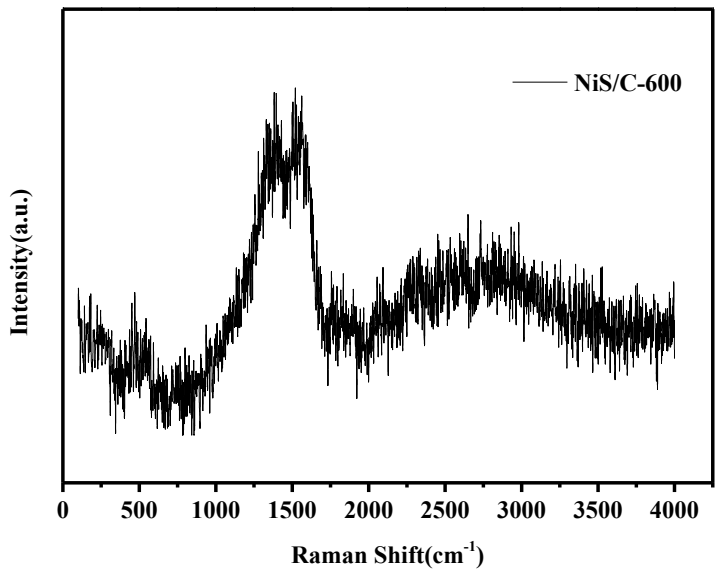

Fig.5. Raman spectra of NiS/C-600.

3.2 Electrochemical properties

The electrochemical performances of the as-prepared NiS nanoparticles, NiS/C-500, NiS/C-600, NiS/C-700 and NiS/C-800 as electrodes for supercapacitor were evaluated in electrochemical workstation. The galvanostatic charge-discharge(GCD) curves of NiS nanoparticles synthesized at different temperatures and reaction times are shown in Fig.6(a-b). The specific capacitance can be calculated according to the following equation:

$$C = \frac{I\mathrm{dt}}{\mathrm{mdv}} \tag{1}$$

where C (F g^{-1}), I (A) , dt (s), m (g) and dv (V) are the specific capacitance, the discharge current, total discharge time, mass of active materials and potential drop during discharge respectively[37]. The specific capacitances of the electrode are 1378.0, 823.2, 1688.5 and 569.8F g^{-1} at 140, 160, 180 and 200°C respectively when the hydrothermal reaction time is 8h. The specific capacitances of the electrode are 625.3, 1688.5, 581.7 and 546.4F g^{-1} at 6, 8, 10 and 12h respectively when the hydrothermal temperature is 180°C. It appears that the specific capacitance increases firstly and then decreases with the increase of reaction time. Obviously, the specific capacitance performance is significantly affected by the hydrothermal reaction conditions. Moreover, the specific capacitance of the NiS nanoparticles are higher than the reported literatures[38, 39] which is attributed to hydrolysis reaction of hexamethylenetetramine(HMTA). In the airtight reaction kettle with high temperatureand pressure, HMTA reacted with deionized water as follows:

$$(CH_2)_6N_4 + 6H_2O \rightarrow HCHO + 4NH_3 \tag{2}$$

$$NH_3 + H_2O \rightarrow NH_4^+ + OH^- \tag{3}$$

Firstly, HMTA plays the role of soft templates as the released HCHO and NH_3 can lead to porous structure. Secondly, the hydroxyl ions will increased with the hydrolysis of ammonia which can promote the hydrolysis of sulfur ions. A series of gently processes can increase the nucleation number and the specific surface area of particles which are consistent with the morphology of the NiS synthesized at 180°C and 8h. Thirdly, HMTA is complexing agent and the slow released ammonia can combine with Ni^{2+} which can control the rate of crystal growth. It is speculated that the porous structure might greatly increase the contact surface area with the electrolyte and favours the electrochemical performances.

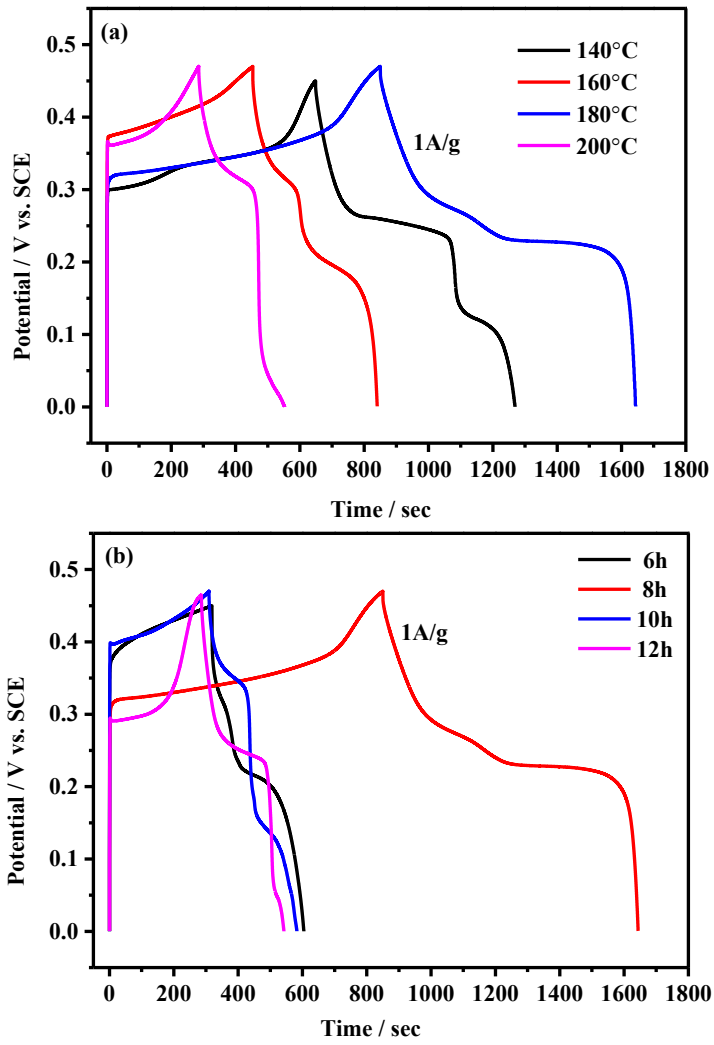

Fig.6. The galvanostatic discharge curves of NiS particles(a) different temperatures from 140°C to 200 °C under the condition of 8h , and (b)different hours from 6 to 12h under the condition of 180 °C at the current density of 1 A g^{-1}.

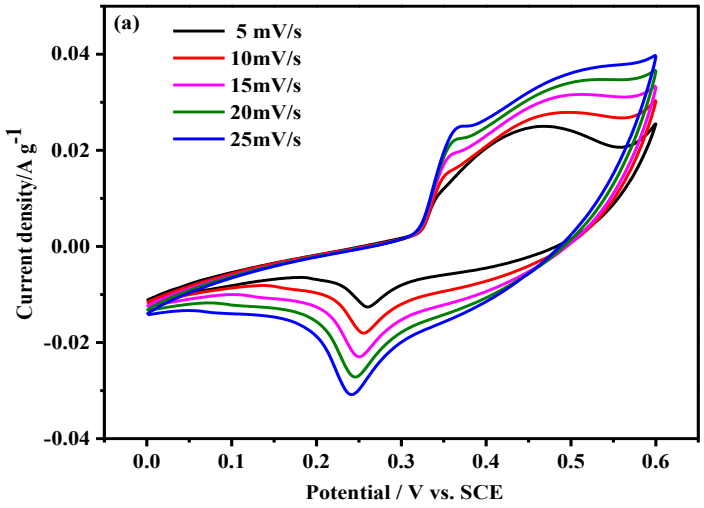
(a)
5 mV/s
10mV/s
15mV/s
20mV/s
25mV/s
Current density/A g-1
0.04
0.02
0.00
-0.02
-0.04
0.0
0.1
0.2
0.3
0.4
0.5
0.6
Potential / V vs. SCE

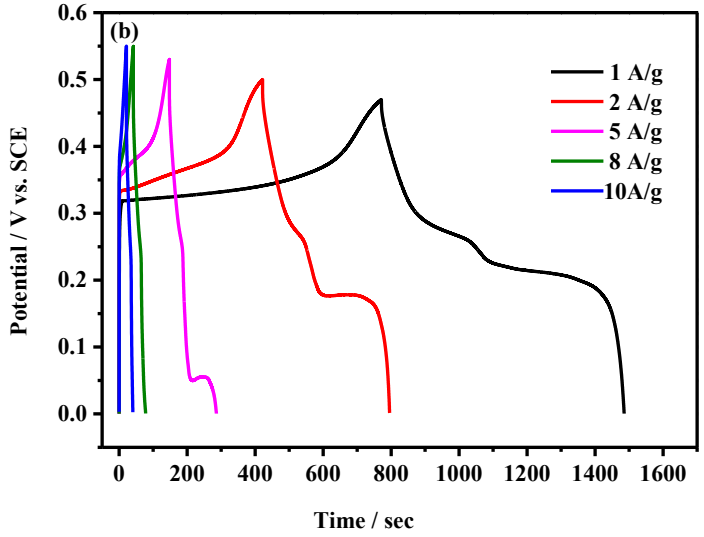
(b)
1 A/g
2 A/g
5 A/g
8 A/g
10A/g
Potential / V vs. SCE
0.6
0.5
0.4
0.3
0.2
0.1
0.0
0
200
400
600
800
1000
1200
1400
1600
Time / sec

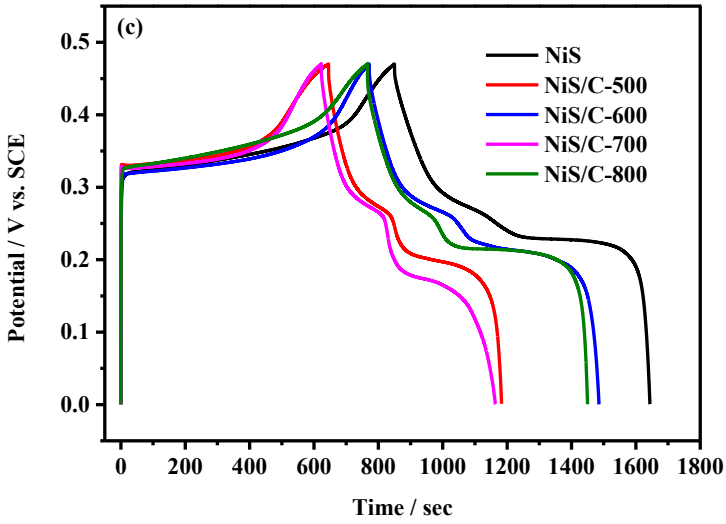
(c)
NiS
NiS/C-500
NiS/C-600
NiS/C-700
NiS/C-800
Potential / V vs. SCE
0.5
0.4
0.3
0.2
0.1
0.0
0
200
400
600
800
1000
1200
1400
1600
1800
Time / sec

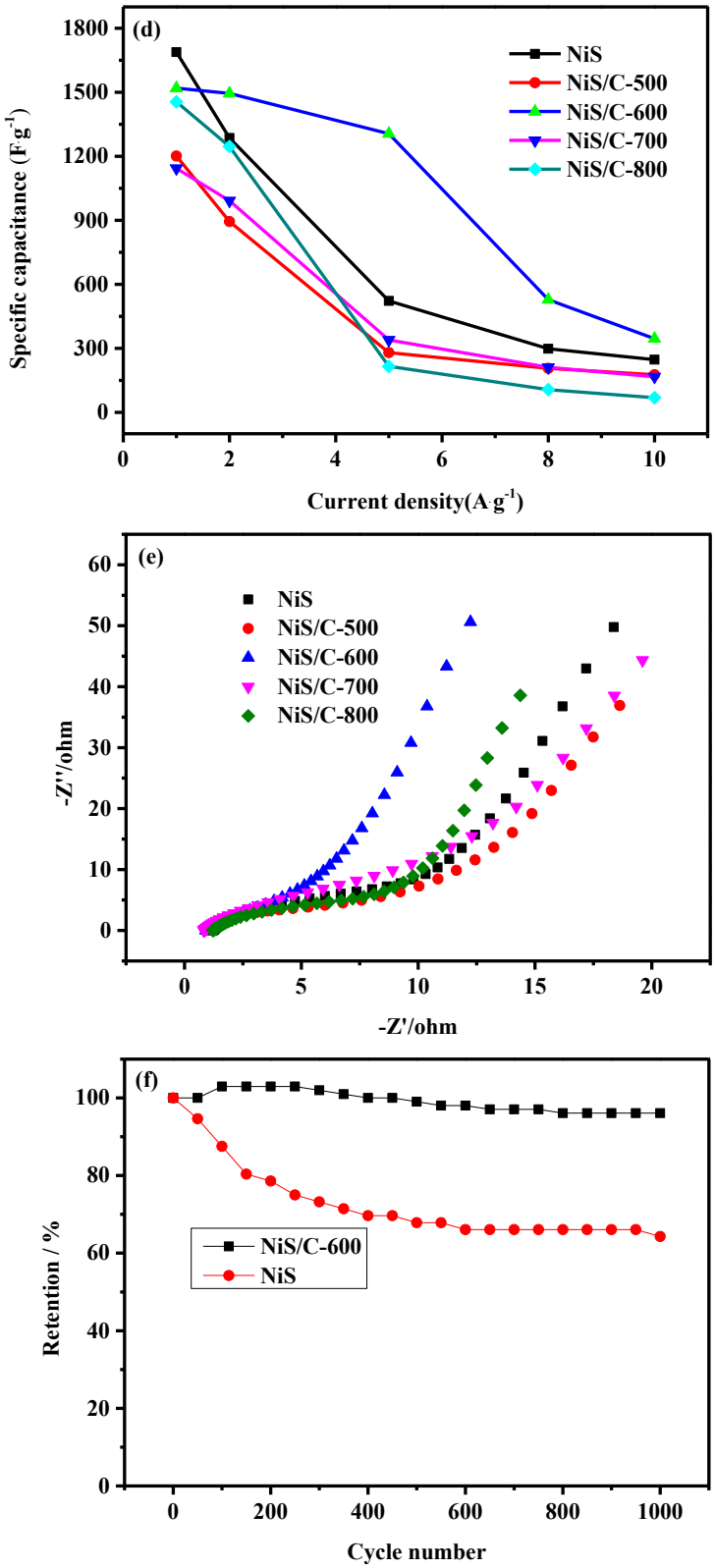

Fig.7. (a) Cyclic voltammetry curves of NiS/C-600, (b) The galvanostatic charge-discharge curves of of NiS/C-600, (c) Specific capacitance of NiS, NiS/C-500, NiS/C-600, NiS/C-700 and NiS/C-800 electrodes at the current density of 1A g^{-1}, (d) Specific capacitance of NiS, NiS/C-500, NiS/C-600, NiS/C-700 and NiS/C-800 electrodes measured as a function of current density, (e)Nyquist plots of NiS, NiS/C-500, NiS/C-600, NiS/C-700 and NiS/C-800 electrodes, (f)Cycling stability of NiS/C-600 electrodes measured at a current density of 5A g^{-1}.

Considering the serious attenuation of specific capacitance in NiS nanoparticles, the walnut shells which have numerous natural channels are selected to increase the electrochemical stability. The cycle voltammetry curves of NiS/C-600 in the 2M KOH aqueous electrolyte with various sweeping rates ranging from 5mV s^{-1} to 25mV s^{-1} are shown in Fig.7(a). In the CV curves, a pair of well-defined redox peaks can be observed obviously, which indicate the presence of a reversible Faradaic reaction and pseudocapacitive behavior. The related reversible reaction can be described as follows:

$$NiS + OH^- \leftrightarrow NiSOH + e^- \quad (4)$$

The anodic peaks at 0.35V and the catholic peaks at around 0.25V correspond to the oxidation and reduction processes respectively. In addition, the oxidation peaks become more positive and the reduction peaks become more negative when the scan rates increase. Moreover, the current density increases correspondingly, which indicates ideal charge–discharge performance for electrochemical energy storage.

The galvanostatic charge/discharge curves of NiS/C-600 at different current densities ranging from 1A g^{-1} to 10A g^{-1} with a potential window of 0 to 0.55 vs. SCE are displayed in Fig.7(b). The nonlinear charge-discharge curves indicate the specific capacitance derives from pseudo-capacitance which match the CV curves very well. The anodic and cathodic peaks at about 0.35 and 0.25V from the CV curves are in accordance with the charge and discharge curves. With the higher current density, the potential window would becomes more wide which is induced by the polarization. When the current density increases, the specific capacitance decreases because the active sites cannot conduct the redox process completely. The galvanostatic charge/discharge curves of the as-prepared NiS nanoparticles, NiS/C-500, NiS/C-600, NiS/C-700 and NiS/C-800 at the current density of 1A $\cdot g^{-1}$ are shown in Fig.7(c) and

the values are 1688.5, 1201.06, 1518.3, 1143.8 and 1455.3F g^{-1} respectively. Obviously, the capacitive performance is excellent compared to other metal chalcogenides. In spite of a slight decrease in capacitance of NiS/C-600, the cycle performance is remarkably improved instead compared to NiS nanoparticles. The specific capacitance(*C*) at various current densities for composites are demonstrated in Fig.7(d). All *C* values decrease with increaseing current densities and the *C* values of NiS/C-600 sheets fade more slowly than others. According to the morphology of the three samples, tremella-like structure of NiS/C-600 composites have the higher effective surface area and more active sites which might be favourable for the accessibility of electrolyte ions and improve the utilization of electrode materials. In contrast, the reunited particles in NiS/C-500, NiS/C-700 and NiS/C-800 block the pores of walnut shells and make these fast ion-transfer channels inaccessible to electrolyte, thus weaken the materials electrochemical performance.

In order to further investigate the electrochemical properties of the three samples, the electron impedance spectroscopy analysis was measured in the frequency range from 100KHz to 0.01Hz which was shown in Fig. 7(e). The Nyquist plot is composed of two parts, the low frequency(R_s) and the high frequency(R_{ct}). The R_s corresponds to the inherent resistance, including the ionic resistance of the electrolyte, the electroactive material and the contact resistance at the active material/current collector interface. It can be seen that the intercepts at the real axis (Z′)of the as-prepared NiS nanoparticles, NiS/C-500, NiS/C-600, NiS/C-700 and NiS/C-800 are 1.217, 0.9443, 0.9261, 0.821 and 1.218Ω. The low R_s values show that the three samples are highly conductive. The lower R_s value of NiS/C-600 can explain the reason why it possesses the higher specific capacitance. R_{ct} represents the Faradic charge transfer resistance. When the slope of the titled curves become higher, the electrolyte ions will transport

to the surface of the electrode materials faster. The NiS/C-600 exhibits largest slope which is associated with its excellent cycling stability. Hence, the addition of walnut shells reduce the impedance and increase the electrical conductivity of NiS, plus improving the ability of circulation in some certains. Figure.7(f) shows the cycle performances of the three electrode materials at a current density of 5A g^{-1}. It can be seen that the capacitance retention of the as-prepared NiS nanoparticles and NiS/C-600 are close to 64.29% and 96.08% after 1000 continuous cycles. To a great extent, the introduction of biomass-derived carbon materials enhance the cycling performance of NiS nanoparticles.

4 Conclusions

In this work, we successfully synthesized the NiS nanoparticles and NiS/walnut shell electrode materials by the facile soft-template hydrothermal method. By adjusting the reaction temperature and time, the uniform NiS particles with a high specific capacitance of 1688.5F g^{-1} at the current density of 1A g^{-1}, good cycling stability and low resistance at the 180°C and 8h are obtained. When the loose and porous walnut shells are employed in the NiS nanoparticles, the obtained NiS/biomass carbon composites not only inherit these excellent characteristics but also improve the electrochemical rate performance and reduce the resistance. Therefore, the NiS/walnut shell composites in this research are promising electrode materials and provide a novel idea for developmental supercapacitor device.

Acknowledgements

This work is supported by Priority Academic Program Development of Jiangsu Higher Education Institutions(PAPD), Top-notch Academic Programs Project of

Jiangsu Higher Education Institutions and the Hong Kong Scholars Program 2016 under Grant No. G-YZ0G.

References

[1] B. Song, J.I. Choi, Y. Zhu, Z. Geng, L. Zhang, Z. Lin, C.-c. Tuan, K.-s. Moon, C.-p. Wong, Chemistry of Materials, 28 (2016) 9110-9121.

[2] K.-J. Huang, L. Wang, J.-Z. Zhang, L.-L. Wang, Y.-P. Mo, Energy, 67 (2014) 234-240.

[3] C.-H. Lai, M.-Y. Lu, L.-J. Chen, J. Mater. Chem., 22 (2012) 19-30.

[4] H. Tang, J. Wang, H. Yin, H. Zhao, D. Wang, Z. Tang, Advanced materials, 27 (2015) 1117-1123.

[5] M. Ciszewski, E. Szatkowska, A. Koszorek, M. Majka, Journal of Materials Science: Materials in Electronics, 28 (2016) 4897-4903.

[6] B. Song, L. Li, Z. Lin, Z.-K. Wu, K.-s. Moon, C.-P. Wong, Nano Energy, 16 (2015) 470-478.

[7] Z. Lu, Y. Chao, Y. Ge, J. Foroughi, Y. Zhao, C. Wang, H. Long, G.G. Wallace, Nanoscale, 9 (2017) 5063-5071.

[8] Y.M. Zhang, Y.W. Sui, J.Q. Qi, P.H. Hou, F.X. Wei, Y.Z. He, Q.K. Meng, Z. Sun, Journal of Materials Science: Materials in Electronics, 28 (2016) 5686-5695.

[9] S. Park, S. Kim, Electrochimica Acta, 89 (2013) 516-522.

[10] L. Pei, Y. Yang, H. Chu, J. Shen, M. Ye, Ceramics International, 42 (2016) 5053-5061.

[11] W. Xiao, W. Zhou, T. Feng, Y. Zhang, H. Liu, H. Yu, L. Tian, Y. Pu, Journal of Materials Science: Materials in Electronics, 28 (2016) 5931-5940.

[12] A.M. Patil, A.C. Lokhande, N.R. Chodankar, V.S. Kumbhar, C.D. Lokhande, Materials & Design, 97 (2016) 407-416.

[13] W. Fu, W. Han, H. Zha, J. Mei, Y. Li, Z. Zhang, E. Xie, Physical chemistry chemical physics : PCCP, 18 (2016) 24471-24476.

[14] G.-C. Li, M. Liu, M.-K. Wu, P.-F. Liu, Z. Zhou, S.-R. Zhu, R. Liu, L. Han, RSC Adv., 6 (2016) 103517-103522.

[15] L. Huang, H. Hou, B. Liu, K. Zeinu, X. Yuan, X. Zhu, X. He, L. Wu, J. Hu, J. Yang, Ceramics International, 43 (2017) 3080-3088.

[16] L. Peng, X. Ji, H. Wan, Y. Ruan, K. Xu, C. Chen, L. Miao, J. Jiang, Electrochimica Acta, 182 (2015) 361-367.

[17] W. Li, S. Wang, L. Xin, M. Wu, X. Lou, J. Mater. Chem. A, 4 (2016) 7700-7709.

[18] Z. Dai, X. Zang, J. Yang, C. Sun, W. Si, W. Huang, X. Dong, ACS applied materials & interfaces, 7 (2015) 25396-25401.

[19] Y. Zhang, W. Sun, X. Rui, B. Li, H.T. Tan, G. Guo, S. Madhavi, Y. Zong, Q. Yan, Small, 11 (2015) 3694-3702.

[20] Z. Li, J. Han, L. Fan, R. Guo, CrystEngComm, 17 (2015) 1952-1958.

[21] S. Li, J. Wen, T. Chen, L. Xiong, J. Wang, G. Fang, Nanotechnology, 27 (2016) 145401.

[22] A. Wang, H. Wang, S. Zhang, C. Mao, J. Song, H. Niu, B. Jin, Y. Tian, Applied Surface Science, 282 (2013) 704-708.

[23] Y. Li, K. Ye, K. Cheng, J. Yin, D. Cao, G. Wang, Journal of Power Sources, 274 (2015) 943-950.

[24] L. Yu, B. Yang, Q. Liu, J. Liu, X. Wang, D. Song, J. Wang, X. Jing, Journal of Electroanalytical Chemistry, 739 (2015) 156-163.

[25] Q. Zhou, C. Jia, X. Ye, Z. Tang, Z. Wan, Journal of Power Sources, 327 (2016) 365-373.

[26] X. Wei, S. Wan, X. Jiang, Z. Wang, S. Gao, ACS applied materials & interfaces, 7 (2015) 22238-22245.

[27] G. Xu, J. Han, B. Ding, P. Nie, J. Pan, H. Dou, H. Li, X. Zhang, Green Chem., 17 (2015) 1668-1674.

[28] Y. Luan, L. Wang, S. Guo, B. Jiang, D. Zhao, H. Yan, C. Tian, H. Fu, RSC Adv., 5 (2015) 42430-42437.

[29] I.I.G. Inal, S.M. Holmes, A. Banford, Z. Aktas, Applied Surface Science, 357 (2015) 696-703.

[30] E.Y.L. Teo, L. Muniandy, E.-P. Ng, F. Adam, A.R. Mohamed, R. Jose, K.F. Chong, Electrochimica Acta, 192 (2016) 110-119.

[31] Y. Li, F. Wang, J. Liang, X. Hu, K. Yu, New J. Chem., 40 (2016) 325-329.

[32] L. Weinstein, R. Dash, Materials Today, 16 (2013) 356-357.

[33] H. Chen, J. Jiang, L. Zhang, H. Wan, T. Qi, D. Xia, Nanoscale, 5 (2013) 8879-8883.

[34] B. Guan, Y. Li, B. Yin, K. Liu, D. Wang, H. Zhang, C. Cheng, Chemical Engineering Journal, 308 (2017) 1165-1173.

[35] B. Song, C. Sizemore, L. Li, X. Huang, Z. Lin, K.-s. Moon, C.-P. Wong, J. Mater. Chem. A, 3 (2015) 21789-21796.

[36] T.-X. Shang, R.-Q. Ren, Y.-M. Zhu, X.-J. Jin, Electrochimica Acta, 163 (2015) 32-40.

[37] W. Chen, D. Gui, J. Liu, Electrochimica Acta, 222 (2016) 1424-1429.

[38] J. Yang, W. Guo, D. Li, C. Wei, H. Fan, L. Wu, W. Zheng, Journal of Power Sources, 268 (2014) 113-120.

[39] X. Yan, X. Tong, L. Ma, Y. Tian, Y. Cai, C. Gong, M. Zhang, L. Liang, Materials Letters, 124 (2014) 133-136.

Figure caption

Fig.1. XRD spectra of NiS at (a) different temperatures from 140^{o}C to 200 ^{o}C under the condition of 8h, (b)different hours from 6 to 12h under the condition of 180 ^{o}C.

Fig.2. SEM images of NiS particles (a-d) different temperatures (140, 160, 180 and 200^{o}C)under the condition of 8h, (e-h)different hours (6, 8, 10 and 12h) under the condition of 180^{o}C.

Fig.3. XPS spectrum of NiS particles (a) XPS survey spectrum, (b)Ni 2p spectrum, (c) S 2p spectrum.

Fig.4. (a-d)SEM images of NiS/C-500, NiS/C-600, NiS/C-700 and NiS/C-800, (e-f)TEM images of NiS/C-600.

Fig.5. Raman spectra of NiS/C-600.

Fig.6. The galvanostatic discharge curves of NiS particles(a) different temperatures from 140^{o}C to 200 ^{o}C under the condition of 8h , and (b)different hours from 6 to 12h under the condition of 180 ^{o}C at the current density of 1A g^{-1}.

Fig.7. (a) Cyclic voltammetry curves of NiS/C-600, (b) The galvanostatic charge-discharge curves of of NiS/C-600, (c) Specific capacitance of NiS, NiS/C-500, NiS/C-600, NiS/C-700 and NiS/C-800 electrodes at the current density of 1A g^{-1}, (d) Specific capacitance of NiS, NiS/C-500, NiS/C-600, NiS/C-700 and NiS/C-800 electrodes measured as a function of current density, (e)Nyquist plots of NiS, NiS/C-500, NiS/C-600, NiS/C-700 and NiS/C-800 electrodes, (f)Cycling stability of NiS and NiS/C-600 electrodes measured at a current density of 5A g^{-1}.